GROWTH OF HIGH QUALITY SILICON MONO INGOTS BY THE APPLICATION OF A MAGNETIC CUSP FIELD IN CZ-PULLER

F. Mosel[1], A. Molchanov[1], Bernhard Fischer[2], Detlef Krischel[2], Albrecht Seidl[3], Bernhard Birkmann[3]
[1] PVA Tepla AG, Im Westpark 10-12, 35435 Wettenberg, Germany
[2] Bruker Advanced Supercon GmbH, Friedrich-Ebert-Str. 1, 51429 Bergisch-Gladbach, Germany
[3] SCHOTT Solar Wafer GmbH, Carl-Zeiss-Str. 4, 63755 Alzenau, Germany

frank.mosel@pvatepla.com, phone: +49 64168690-125, fax: +49 64168690-822

ABSTRACT: The quest for the improvement of solar cell efficiency and a reduction of production costs was the intention for the joint project. The aim of this project is to work out the potential of the magnetic Czochralski technology as a process control system for the crystal quality, the process stability, material parameters and the performance of the solar cells in an industrial scale. Therefore a superconducting magnet in a cusp configuration (Bruker ASC GmbH) was installed on a Czochralski puller (PVA Tepla AG) for the growth of silicon mono crystals. Boron doped crystals were grown under various growth conditions for the production of full square 6 inch p-type wafers. These wafers were used for the characterization of the material parameters especially with respect to the oxygen content and were processed to standard (Al-BSF) and PERC solar cells (Schott Solar AG) for the evaluation of the cell parameters. It is experimentally confirmed that the suitable application of a cusp magnetic field increases process stability and allows a higher growth rate while simultaneously decreasing the oxygen content in the crystals significantly. It is shown that solar cells produced from these crystals show higher cell efficiency as well as smaller LID.

Keywords: c-Si, Czochralski, Degradation, MCZ, Oxygen

1 INTRODUCTION

The fact that semiconductor melts are electrically conductive opens the possibility of using magnetohydrodynamic effects to influence the melt motion which is driven by buoyancy and forced convection and to some extent by Marangoni convection. Especially in the case of large melt volumes, the melt flow is turbulent and the application of static magnetic fields is used to damp these melt instabilities to grow reproducibly large silicon crystals corresponding to the demands of the semiconductor industry. The technology of applying magnetic fields during the growth is well established as the Magnetic Czochralski (MCZ) technology.

Nowadays this technology is coming into the focus of the PV industry for the growth of monocrystalline silicon crystals, because the main challenges of the market are a dramatic reduction of the production costs and a further improvement of the solar cell efficiency. These demands require an increase of the process yield in terms of higher melt volumes and faster pull rates as well as the reduction of impurities, in particular the content of oxygen which is the principal factor for the formation of crystal defects acting as recombination centers in Czochralski silicon [1, 2].

The application of a CUSP field seems to be favorable because it offers the possibility to combine the magnetic field distributions of a horizontal and a vertical magnetic field. About the effects of the different magnetic field configurations (horizontal, vertical, CUSP) on the heat and mass transport in the melt during the crystallization a lot of numerical simulation work is present in the literature [3, 4]. However, only a few real comparisons of numerical results with experimental work are known, e.g. on the oxygen distribution in the crystals grown under different field applications. Therefore it was decided to perform a complete investigation about the influence of a CUSP magnetic field during the crystal growth process via the material parameters on the cells which were fabricated from these ingots.

Figure 1: MCZ ingot, dia. 225 mm, $\rho = 3 - 1.5\ \Omega$cm, grown at PVA TePla AG by use of a superconducting coil system from Bruker ASC.

2 EXPERIMENTAL

2.1 Crystal Growth Apparatus

For the crystal growth experiments a Czochralski puller EKZ 3500 from PVA Tepla AG was used. This machine is designated for the use of magnetic systems and was equipped with a cryogen-free superconducting CUSP magnet system from Bruker ASC. As a so-called “dry system” it is very economical because it does not need any cryogenic liquid as a cooling medium. The power consumption is about 10% compared to a resistive copper conductor based magnet [5]. The CUSP field is generated by two axial coils which produce opposite fields. The magnet is completely integrated in the process control system of the EKZ 3500. The magnetic field configuration can be varied by the magnitude and the ratio of the currents in the two coils during the process and is controlled automatically. In this way also vertical asymmetric fields can be generated by an unequal current ratio. Fig. 2 shows the magnetic field pattern in a vertical plane, the crucible is indicated by black lines.

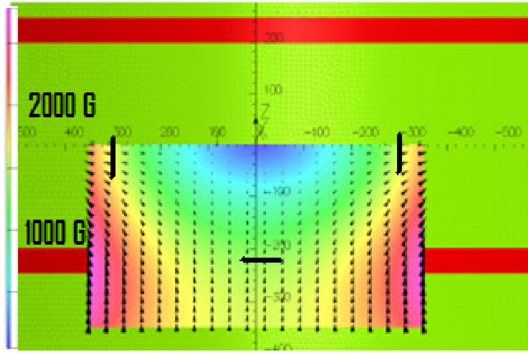

Figure 2: Magnetic field pattern in the lower half plane of the symmetric CUSP – field for an induction current of 135 A. The lines indicate the border of the crucible with a magnetic induction of 1500 G at the bottom and 1300 G at the melt surface at the crucible rim.

2.2 Crystal Growth Experiments

The crystal growth experiments were performed under the perspective of crystal quality, e.g.: cell efficiency and process stability. Regarding the crystal quality 9 boron-doped silicon crystals of <100> orientation were grown in a 24 inch hot zone. The crucibles were made from synthetic quartz with a doped inner layer. The initial conditions with the exception of the magnetic field conditions and crucible rotation rate were identical for the growth runs MCZ1 – MCZ 9. The initial charge was 120 kg solar grade polysilicon with a purity of n > 100 Ωcm and p > 1000 Ωcm. The crucible position and its variation during the growth was the same for all crystals. The pulling speed was 1.0 mm/min. The argon flow conditions were also identical. The differences of the magnetic field conditions of the growth runs are the position of the symmetric plane of the CUSP field with respect to the melt level and the strength of the magnetic field induction. In all cases the CUSP field was symmetric, that is the currents of the two coils were the same. The position of the so-called “CUSP plane” was varied by the position of the CUSP magnet via a lifting system. Figure 3 shows the different positions of the CUSP plane. During the growth process the distance of the melt level with respect to the CUSP plane was held constant automatically by a control loop.

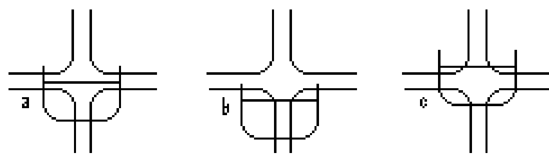

Figure 3: CUSP plane configurations relative to the melt level: a) CUSP plane on melt level, b) CUSP plane in the growing crystal, c) CUSP plane in the melt

Three crystals were grown with different crucible rotation rates under different magnetic field conditions to investigate the interaction of the forced convection due to crucible rotation rate with the magnetic field. Tab. 1 summarizes the field configurations and the rotational conditions of the growth experiments.

The growth experiment MCZ V was a special growth run to check the influence of the CUSP field on the critical pulling rate for the onset of twisting and compared to our standard growth conditions. Therefore the crystal was grown with the standard diameter of 205 mm and compared to previous high speed experiments.

	field configuration		rotational conditions	
Ingot	current [A]	CUSP-plane	crucible	crystal
MCZ 1	0	ml	10	-10
MCZ 7	0	ml	10	-10
MCZ 2	135	ml	10	-10
MCZ 8	135	ml	10	-10
MCZ 3	135	ml - mh/3	10	-10
MCZ 4	135	ml + mh/6	10	-10
MCZ 6	80	ml	5	-10
MCZ 5	135	ml	5	-10
MCZ 9	135	ml	2	-10
MCZ V	100	ml	10	-10

Table 1: The magnetic field configuration is characterized by the induction current [A], which is identical in both coils. The position of the CUSP plane: “ml” means CUSP plane on melt level, “ml – mh/3” means CUSP plane 1/3 of the initial melt height below melt level, “ml + mh/6” means CUSP plane 1/6 of the initial melt height above melt level.

The magnetic field was applied after the melting process and a certain time of melt stabilization. With increasing field intensity the melt surface became calmer resulting in a very smooth and shiny surface of the grown ingot (see fig. 1). After growth the cool down procedure was identical for all crystals with regard to the formation of thermal donors. The crystals with a diameter of 225 mm had a length of 1130 mm.

Out of the grown 9 ingots, 6 are already examined and will be analyzed within this paper.

2.3 Analysis of the grown crystals

The crystallized ingots were wafered in a standard production environment by multi-wire sawing using a SiC-based slurry. All wafers were lasermarked in order to be able to retrieve the original position of the wafer in the ingot. The specific resistivity was measured by the eddy current method. The defect characteristics were revealed by MWPCD lifetime measurements and photo-luminescence imaging on as cut wafers [6] and on finished solar cells. The interstitial oxygen and substitutional carbon content were determined by means of FTIR spectroscopy. The conversion factors were 3,14 x 10^{17} atoms/cm^3 at wave number 1107 cm^{-1} [O_i] and 0,82 atoms/cm^3 [C_s] at wave number 605 cm^{-1} according to SEMI MF 1188-1107 and 1391-1107.

Selected wafers were processed to either

a) standard solar cells using alkaline texturing, POCl-diffusion and an Al-BSF or to

b) PERC cells, for which the backside obtained an additional passivating layer [7].

For the PERC process, an additional reference group (10 pcs.) of commercially available “high quality” wafers with the following properties (ρ=2,5 Ωcm, [O_i]=11x$10^{17}$$cm^{-3}$) was added.

The finished cells were tested for light induced degradation (LID). In this procedure the cells were exposed to a light intensity of 400 W/m^2 for a duration of up to 140 h at an elevated temperature of 55°C.

3 RESULTS

3.1 Crystal Growth

The ingots had a length of 1130 mm and a weight of ~ 115 kg. With the exception of MCZ 6 all crystals were complete monocrystalline from top to tail. Unfortunately ingot MCZ 6 underwent a structure loss at a bodylength of 810 /1130 mm. The total body yield for all crystals was 97%. The uniformity of the diameter in the cylindrical part of the body is shown in fig. 4. The setpoint diameter is 225 mm. The whiskers in the boxplot indicate the minimum and maximum values of the diameter. The crystals which were grown with reduced crucible rotation rates exhibit excellent diameter control due to the melt stabilizing effect of the magnetic field.

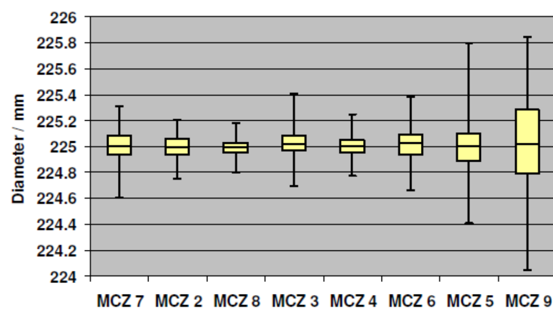

Figure 4: Boxplot of the diameter distribution in the main part of the body measured by the optical diameter detection system.

3.2 Raw Wafer Analysis

Fig. 5 shows the axial variations of the resistivity for the evaluated crystals grown in the series of experiments. With the exception of MCZ3 the specific resistivity of all crystals is in the scheduled range of 3 to 1 Ωcm. The specific resistivity is inversely proportional to the boron concentration. The large deviation of the resistivity of MCZ 3 from the target value is attributed to the presence of thermal donors. This is discussed in detail in Sec. 4.3. The axial oxygen concentration for the different magnetic field configurations is shown in fig. 6. The crystals grown with the CUSP plane on the melt level and the CUSP plane above the melt level exhibit a lower oxygen concentration which is about half compared to the crystal grown without magnetic field application.

Crystal MCZ 6, for which the field strength was halved, reveals an oxygen content in between the reference and the ingots grown in maximum magnetic field.

The crystal MCZ 3 which was grown with the CUSP plane below the melt level shows a significantly higher oxygen concentration. The carbon content is in the same range of 2 – 5 x 10^{16} atoms/cm^3 for all crystals and is homogeneously distributed along the crystal length.

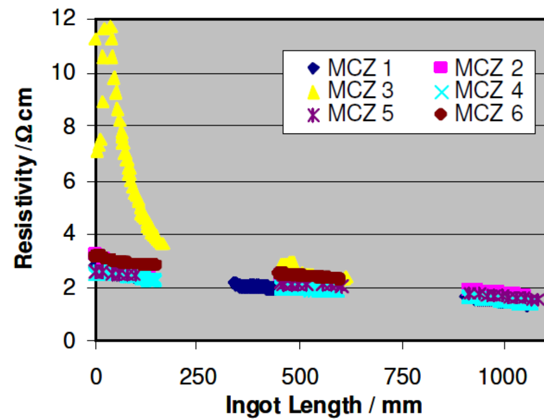

Figure 5: Variation of the wafer resistivity along the axis of the ingots. The high resistivity of MCZ 3 in the first part results from a large number of thermal donors.

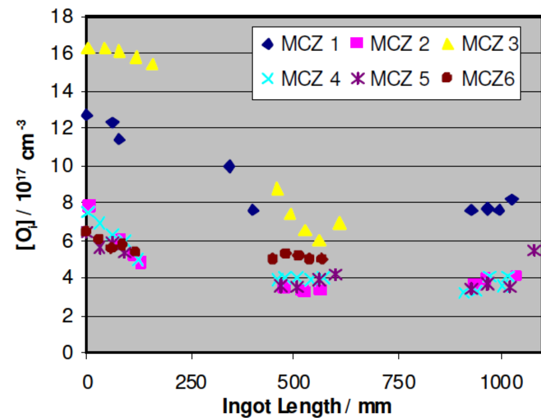

Figure 6: Variation of the interstitial oxygen content O_i along the axis of the ingots. Except for MCZ 3 the CUSP field effectuates a reduction of the oxygen content about the half in comparison to the reference ingot (MCZ 1).

3.3 Solar Cell Results

All standard solar cells manufactured from wafers with $[O_i] < 8x10^{17}$ cm^{-17} showed efficiencies (18,6…18,7%), at the upper edge of the process window whereas standard material only reached values of 18,5%. However as the MCZ-wafers were processed in different runs, their efficiencies can not be compared directly, as process to process variations have a similar order of magnitude.
This problem was circumvented in case of the PERC cells where all cells were processed within the same run. The achieved efficiencies are given in fig. 7 as a function of the oxygen content.

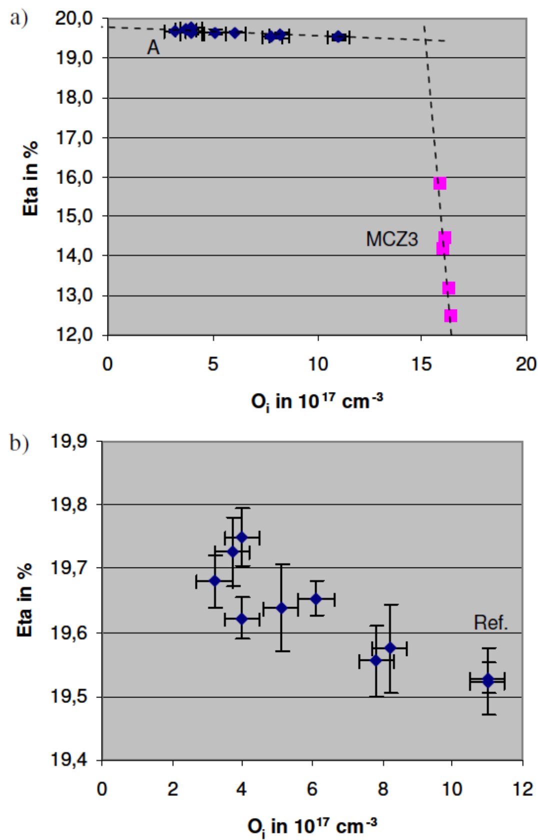

Figure 7: a) Variation of the PERC Eta with oxygen content. Please note that the points named MCZ 3 are single values/cells, whereas the points named A are always averages of 5 to 8 cells. The dashed lines are a guide to the eye. b) enlarged section of A. The points named Ref. are either from the commercial or internal standard (MCZ1).

It turns out that there is an increase of efficiency with decreasing oxygen content. This increase can be up to 0,2…0,3% absolute in comparison to the reference groups. When the O_i content comes close to $15x10^{17}$ cm^{-3}, a sudden (wafer-related) breakdown of the cell efficiency occurs. In order to examine this breakdown in more detail PL-pictures of the cells have been made (fig. 8).
Apart from a very interesting striation structure, Fig. 8a shows that MCZ 3 has a strongly reduced PL intensity in the center of the cell. This is expressed very clearly in Fig. 8c, where the intensity profiles along one diagonal of the cells are compared. As both wafers are coming from a comparable ingot height the base doping level is also comparable and the PL intensity is proportional to the effective lifetime.

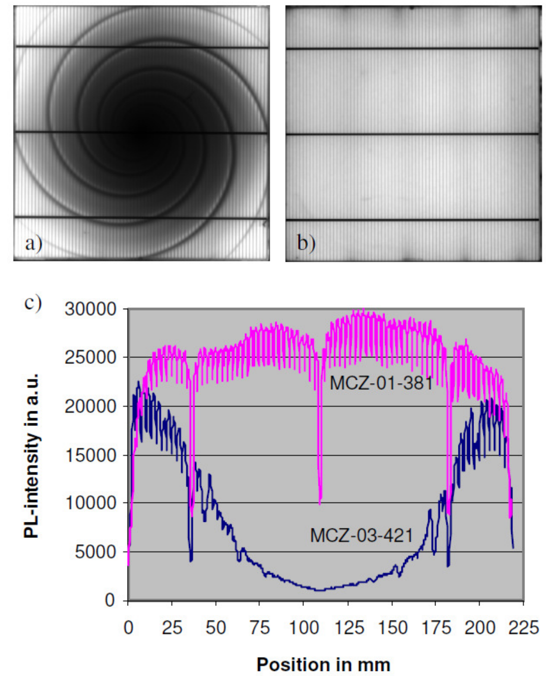

Figure 8: a) PL-images of Al-BSF-Cells MCZ-03-421 and b) MCZ-01-381. The dashed line indicates the diagonal along which the PL intensity profiles in c) were taken.

3.4 Light induced degradation (LID)

The cells are degraded according to the conditions given in Sec. 2.3. The results are shown in fig. 9.

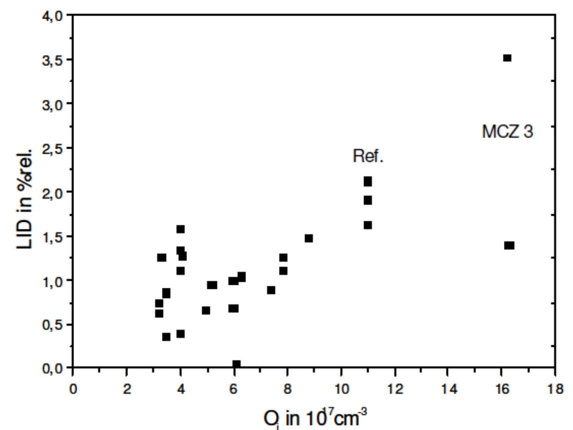

Figure 9: rel. LID of PERC-Cells as a function of the oxygen content. The reference and the cells from the high efficiency region of MCZ 3 are explicitly marked.

It can be recognized that there is indeed a trend to higher LID for increasing oxygen content as this is expected. Nevertheless for $[O_i] < 10 \times 10^{17}$ cm^{-3} the LID is below 2% which is generally considered as acceptable value.

4 DISCUSSION

4.1 Crystal Quality

During the growth process the silica crucible is dissolved by the silicon melt with an erosion rate of

approximately 7 µm/h [8]. Most of the oxygen evaporates as SiO from the melt surface. Only a small amount of the oxygen supplied from the crucible (< 1%) is incorporated in the growing crystal. The oxygen concentration in the melt is determined by the surface area of the crucible wetted by the silicon melt and the evaporation rate of SiO(g) which is limited by the area of the free melt surface. This balance determines the oxygen concentration in the crystal. In the melt volume the oxygen concentration is almost homogeneous due to the strong convective mixing. Concentration gradients of oxygen exist in the transition regions from the crucible wall to the melt, from the melt to the atmosphere and from the melt to the crystal.

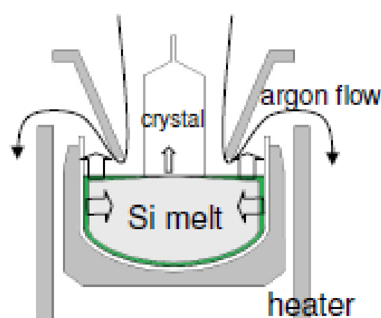

Figure 10: Diagram of the oxygen transport in Czochralski Silicon growth

These areas of exchange can be described as diffusion controlled boundary layers [9, 10]. The extension of the layers is influenced by the convective flow regimes in the melt and also by the gas flow conditions on the free melt surface. A decrease of the thermal convection especially near the crucible wall increases the thickness of the diffusion layer and hence slows down the dissolution rate of the crucible wall.

The damping effect of the CUSP-field on the melt flow is very effective where the magnetic field components are perpendicular to the melt flow.

In the set of experiments three different positions of the CUSP field have to be considered.

The CUSP plane is at the growth interface (see fig. 3), that means that in the melt volume vertical components of the magnetic field are predominant whereas at the melt surface horizontal field components are effective at the crucible periphery. The influence of the CUSP field on the melt flow in the area underneath the crystal is low. That means that the boundary layer at the crystal melt interface is scarcely influenced by the magnetic field when the CUSP plane is at the growth interface.

A position of the CUSP plane in the melt enhances the horizontal character (see fig. 3) of the magnetic field in the melt volume, whereas a CUSP plane above the melt effectuates a vertical magnetic field configuration in the melt volume and on the crystal melt interface.

The oxygen concentrations in the crystals grown under horizontal dominated CUSP field conditions at the melt surface are different from the crystal grown under vertical dominated CUSP field [11]. Compared to the reference crystal grown without CUSP field our experiments show that a CUSP plane at the melt surface or slightly above the melt is preferable to a CUSP plane below the melt which leads to an increased oxygen incorporation. This means that in the latter case the diffusion boundary layer at the crystal-melt interface is strongly influenced by magnetic field components resulting in an increased oxygen distribution in the crystal, especially at the top of the ingot. Also the oxygen transport in the atmosphere may be inhibited by an increased boundary layer at the gas interface.

The effect of the crucible rotation rate on the oxygen distribution under the action of a CUSP field with its plane at the melt surface seems to have a negligible influence for a reduction from 10 to 5 rpm under the applied growth conditions (see tab.: 1 and fig.: 6). The crystal grown with a crucible rotation rate of 2 rpm is still under evaluation.

These different CUSP plane configurations of the experiments have no appreciable effect on the axial redistribution of the boron. The dopant shows the classical segregation distribution of a batch solidification process with a segregation coefficient of k_{eff} ~0.8 [10]. The boron concentrations in the crystals can be deduced from the specific resistivity distribution (fig.: 5).

4.2 Process Stability

It is shown by numeric simulations [5] and also experimentally proven [12] that under the influence of static magnetic fields higher growth rates are achievable. Also the position of the CUSP plane seems to have an influence on the critical pull rate at which twisting starts [12]. Therefore we performed one growth experiment with the CUSP plane at the melt surface which is the best configuration in our growth conditions with respect to the oxygen content in the crystals. Compared to our standard configuration without magnetic field application we achieved with this first experiment stable growth conditions which permit a higher pull rate of 15 %.

We observed also in all crystals grown under magnetic field an absolute smooth and shiny crystal surface with an improved diameter constant in the body. Exceptional cases were the crystals grown under reduced crucible rotation (see tab.: 1 and fig.: 4). Here the diameter variations are more pronounced but still negligible.

4.3 Special Discussion of MCZ 3

MCZ3 is a very interesting ingot. In this case the CUSP plane was below the melt level. The large difference between target and reached resistivity is indeed caused by a large amount of thermal donors. This was proven by annealing experiments in which the donors were destroyed and the resistivity indeed reached its targeted value. The high thermal donor concentration goes along with a high concentration of interstitial oxygen. The initial formation rate and the maximum concentration of thermal donors are known to depend in the 4th and 3rd order of the O_i-content [13].

Taking a close look at fig. 6, it seems that the $[O_i]$ is saturating close to the ingot shoulder of MCZ 3. This is indeed expected as the total oxygen concentration in the crystal is much higher and the $[O_i]$ is only the part which has not precipitated. From fig. 6 it can be deduced that the critical $[O_i]$ is close to $15x10^{17}$ cm^{-3}. Sabatino et al. [14] show a similar effect in mc UMG Si, although their $[O_i]$ ($12{,}5$ $x10^{17}$ cm^{-3}) is slightly lower. But this might be process- and material- related.

From the PL images (fig. 8) it can be deduced that the oxygen precipitation occurs in this case mainly in the centre of the cells. Indeed the pictures are very similar to

results of Haunschild et al. [15]. When the PL intensity is interpreted as effective lifetime then findings indicate a dramatic loss of lifetime larger than one order of magnitude in the wafer center. This also explains the low efficiency in the case of MCZ 3.

4.4 Discussion of the Cell Results and the LID

The results achieved indicate that it is essential to work on a reduction of the $[O_i]$ content in CZ-ingots. For PERC cells there is indeed a significant efficiency gain.

Looking at the LID values, they are also very low. For reasons of clarity we have plotted them versus $[O_i]$. According to Bothe et al. [16] they should be plotted against $[B]^{0,824}$ x $[O_i]^{1,748}$ as also Boron is involved in the formation of this complex. As our doping range is very small and as $[O_i]$ enters nearly quadratic fig.9 in fact remains unaffected.

5 CONCLUSIONS

The results give an experimental evidence of the influence of a magnetic CUSP field on the incorporation of oxygen in silicon crystals during Czochralski crystal growth. The amount of oxygen distributed in the crystals depends mainly on the position of the CUSP field relative to the melt and the strength of the magnetic induction. A reduction of the oxygen content by about half is shown. The axial redistribution of boron in the crystals, estimated by the specific resistivity, shows no marked effect due to its effective distribution coefficient of k_{eff} ~ 0.8.

The halving of the oxygen content has a positive impact on the LID. A LID below 1 % is possible.

A further decrease of the oxygen content by the application of higher magnetic induction during the crystal growth seems to be possible. Also further improvements of the standard growth parameters e.g. crucible rotation rate and optimized argon flow are under investigation.

Additionally the CUSP field has a positive impact on production yield. An increase of the pulling speed of 15% is demonstrated.

It can be anticipated that future types of solar cells with efficiencies beyond 20% will be even more sensitive to lifetime affecting defects. Therefore the need for silicon with low oxygen content will increase even further. MCZ offers a unique solution to this task.

6 REFERENCES

[1] J. M. Hwang, D. K. Schroder, J. Appl. Phys 59 (7) (1986) 2476.

[2] J. B. Murphy, K. Bothe, M. Olmo, V. V. Voronkov, R. J. Falster, J. Appl. Phys 110 (2011) 053713-1.

[3] H. Yu, Y. Sui, J. Wang, F. Zhang, X. Dai, J. Mater. Sci. Technol., 22 (2) (2006) 173.

[4] Y. Huiping, J. Wang, Y Sui, X. Dai, G, An, Chinese J. Chem. Eng.,14 (1) (2006) 8.

[5] A. de Potter, V. Regnier, B. Fischer, D. Krischel, Proceedings 25th European Photovoltaic Solar Energy Conference, Valencia, Spain, (2010) 1517.

[6] B. Birkmann, A. Hüsler, A. Seidl, K. Ramspeck, H. Nagel, Proc. 26th European Photovoltaic Solar Energy Conference, Hamburg, Germany, (2011) 937.

[7] Schott Solar Press Release, 25.11.2011.

[8] W. Zulehner, d. Huber, J. Grabmeier (Ed.), Crystals 8, Silicon, Chemial Etching, Springer, Berlin (1982)

[9] K. Hoshikawa, X. Huang, Materials Science and Engineering B72 (2000) 73.

[10]P.J. Ribeyron, F. Durand, Journal of Crystal Growth 210 (2000) 541

[11]R.W, Series, Journal of Crystal Growth 97 (1989) 85

[12] W.von Ammon, Yu. Gelfgat, L. Gorbunov, A. Mühlbauer, A. Muiznieks, Y. Makarov, J. Virbulis, G. Müller, Proceedings of the 15th Riga and 6th PAMIR Conference on fundamental and applied MHD, (2005) 41

[13]F. Shimura (Ed.), Oxygen in Silicon, Academic Press.

[14]M. Di Sabatino, S. Binetti, J. Libal, M. Acciarri, H. Nordmark, E. J. Øvrelid, Sol. En. Mat. & Sol. Cells 95, (2011) 529.

[15]J. Haunschild, J. Broisch, I. E. Reis, S. Rein, Proc. 26th European Photovoltaic Solar Energy Conference, Hamburg, Germany, (2011) 937

[16]K. Bothe, R. Sinton, J. Schmidt, Prog. Photovolt: Res. Appl. 13 (2005) 287